atmosphere

MDPI

Article

Influence of Atmospheric 10–20 Day Low Frequency Oscillation on Regional Strong Cooling Events in the Winter of Northern China over the Past 40 Years

Wei Zhang [1], Liping Li [1,*] and Jinghua Ren [2]

[1] Key Laboratory of Meteorological Disaster of Ministry of Education (KLME), Collaborative Innovation Center on Forecast and Evaluation of Meteorological Disasters (CIC-FEMD), Nanjing University of Information Science and Technology, Nanjing 210044, China
[2] Xinhe Meteorological Bureau, Aksu 842100, China
* Correspondence: llp@nuist.edu.cn

Abstract: Using daily minimum temperature data at 2481 stations provided by the National Meteorological Information Center (China) and the daily reanalysis data from NCEP/NCAR during the period from 1980 to 2019, the effects of atmospheric low frequency oscillations (LFOs) on the regional strong cooling events (RSCEs) in the winter of northern China are investigated, and the extended range forecast signals of the RSCEs are extracted. The results show that: (1) The frequency of RSCEs is higher before the year 2000 and then decreases, but its interannual variability increases. There are 10–20, 20–30 and 30–60 d significant low frequency periods in the regional average minimum temperature in northern China, and the low frequency oscillation with a period of 10–20 d is the most significant. (2) The low frequency key systems affecting RSCEs in the west, middle, and east of northern China are the Ural blocking high and the trough of Lake Balkhash-Baikal (Lake Ba-Bei), the blocking high in the northwest and the low trough in the southeast of Lake Ba-Bei, the Lake Ba-Bei blocking high and the East Asian trough, respectively, and the Siberian High (SH) that expands and moves with the blocking high all the time. The low frequency jets at the upper level are weaker in the north and stronger in the south. (3) The low frequency high potential vorticity (PV) center in the lower stratosphere moves eastward and southward along the 315 K isentropic surface via the north of Lake Ba-Bei, southern Lake Baikal and Northeast China to the Sea of Japan, causing the 2 PVU line to move southward and then the above-mentioned high PV center in the mid-high troposphere to extend vertically. Meanwhile, under the influence of gradually increasing upper level jets and vertical meridional circulation, the high PV column continues to propagate downward to the mid-low troposphere at lower latitudes along the 300–315 K isentropic surfaces, which enhances the low frequency positive vorticity and deepens the key trough. In addition, the convergence in the upper troposphere, the divergence in the lower layer, and the development of descending motion behind the trough lead to the development and southward movement of the SH. (4) At −10 d, the positive and negative low frequency anomalies at 500 hPa geopotential height appearing in the East European Plain and Western Siberian Plain are the extended range forecast signals for RSCEs in the winter of northern China, respectively.

Keywords: regional strong cooling events; atmospheric low frequency oscillation; cold air source; extended range forecast signals

Citation: Zhang, W.; Li, L.; Ren, J. Influence of Atmospheric 10–20 Day Low Frequency Oscillation on Regional Strong Cooling Events in the Winter of Northern China over the Past 40 Years. *Atmosphere* **2022**, *13*, 1406. https://doi.org/10.3390/atmos13091406

Academic Editor: John Walsh

Received: 13 July 2022
Accepted: 30 August 2022
Published: 31 August 2022

1. Introduction

According to the sixth special report of the Intergovernmental Panel on Climate Change (IPCC) [1], the frequency, intensity and strength of extreme weather and climate have been increasing worldwide in the context of global warming. Since 1970, the frequency of winter cold waves in China has generally shown a decreasing trend [2–5], but it has increased slightly again since 2009 [6]. In addition, the interannual variability of its frequency

and intensity increases, leading to increased extremes of events [7] and posing serious threats to the social economy and people's lives and property [8,9]. By now, a relatively systematic and classic cold wave theory has been developed [10,11]. The large-scale southward intrusion of strong cold air in the mid-high latitude of the northern hemisphere can initiate a cold wave. The cold air from the source is the entity of the cold wave process, and the circulation patterns such as the large-scale trough or ridge, blocking systems, the Siberian High (SH) and winter monsoon are all the carriers of cold air. That is, the moving path of the circulation systems is the propagation path of cold air [12]. In winter, when the blocking ridge on the east of the Ural Mountains is established and its downstream horizontal trough turns vertically, then it couples with the southern branch trough to reconstruct the East Asian trough, eventually leading to a strong cold wave outbreak [13]. The combined effects of the abnormally strong SH and Aleutian Low (AL), the stable maintenance of the Ural blocking high in the mid-troposphere, and the enhanced winter monsoon due to La Nina events can lead to abnormally cold winter events [14,15]. Among them, the cold air activity caused by the development and southward movement of the SH in winter can directly affect the winter temperature in China, with a significant negative correlation between the intensity of the SH and the winter temperature [2,16,17]. Moreover, the enhanced 500 hPa Eurasian ridge can favor the development of the SH. When the SH is more powerful and extends southeastward, the winter is colder [18,19]. The strength and location of the Asian upper level jets are also essential factors that can affect temperature change in winter in China [20–22]. When the upper level jets are weak in the north and strong in the south, the cold air from high latitude moves actively southward and the East Asian trough is deepened, resulting in widespread low temperatures in central and eastern China [6,19].

Anomalies in atmospheric circulation frequently cause large-scale extreme weather and climate, while atmospheric low frequency oscillations (LFOs) also play an important role in the evolution of weather and climate, particularly in the occurrence of periodic, persistent, extreme, and high-impact events [23]. Atmospheric low frequency variability mainly consists of 30–60 d intra-seasonal oscillation and 10–20 d quasi-biweekly oscillation [24]. The Rossby wave, which is caused by intra-seasonal oscillations in the tropical atmosphere, causes air to descend abnormally through the meridional vertical circulation, affecting the range and path of cold air in the extratropical atmosphere [25–27], as well as the winter climate in China [28–30]. It is found that the representative factors of cold air intensity, such as land surface temperature or air pressure, and mid-high latitude circulation systems in the northern hemisphere (for instance, the polar vortex, the SH, the East Asian trough, the AL and northeastern cold vortex, as well as the East Asian winter monsoon) all exhibit distinct LFO characteristics [13,31,32]. There are mainly 10–20 d and 30–60 d LFO in winter temperatures in China [33–35]. Two 10–20 d low frequency wave trains exist to the north and south of 40° N and couple, contributing to the outbreak of a nationwide cold wave [12]. The close coupling of low frequency fluctuations at mid-high latitude in the northern hemisphere can lead to the occurrence of extreme cold events in winter either nation-wide or in various regions such as the Northeast China, North China, and South China [26,36–39].

In summary, the influence of interannual atmospheric circulation anomalies on strong cooling events (SCEs) has already been systematically studied. There are also some studies on the impact of atmospheric LFO on SCEs, but most of them are analyzed for individual events, and some differences exist in the impact of atmospheric LFO on SCEs in different regions. Northern China, spanning 16 provinces (regions) in the Northwest China, North China and Northeast China, is significantly affected by SCEs. In order to achieve the Sustainable Development Goals—UN 2030 agenda [40–42], specifically to reduce economic damage to agriculture in northern China so as to guarantee sustainable agricultural development and stable economic development under the influence of extreme events, and to be able to issue timely cooling warnings and take emergency action to ensure a healthy and safe life for society at large, the influence of atmospheric LFO on the regional strong cooling events (RSCEs) in the winter of northern China will be investigated during the period from

1980 to 2019 in this paper, and extended-range forecast signals will be extracted to provide the reference for improving the accuracy of seasonality and medium-term forecasts of extreme events in northern China and for addressing global climate change and its impacts.

2. Data and Methods

2.1. Data

The data include (1) daily minimum temperatures at 2481 stations provided by the National Meteorological Information Center (China); (2) global daily reanalysis data including geopotential height field, temperature field, and wind field, provided by the United States National Centers for Environmental Prediction/National Center for Atmospheric Research (NCEP/NCAR) (NCEP/NCAR Reanalysis 1: NOAA Physical Sciences Laboratory) with a horizontal resolution of 2.5 × 2.5° [43]. The data period is from 1980 to 2020. The winter is defined from December to February of the following year. The north of 35° N is defined as northern China in this paper. To ensure the continuity and integrity of data, excluding the stations with missing data or insufficient time length, 903 stations are finally selected. The distribution of the stations is shown in Figure 1.

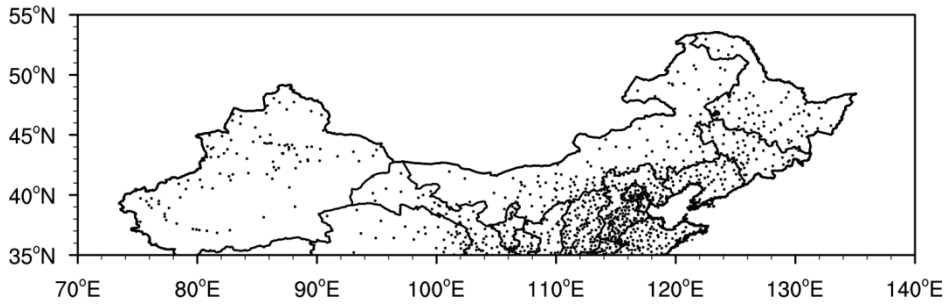

Figure 1. Distribution of 903 stations in northern China.

2.2. Methods

2.2.1. Definition of RSCE

First of all, based on the regulations of "Cold Wave Level" (GB/T21987-2017) and "Cold Air Level" (GB/T20484-2017) published by the National Meteorological Center of China Meteorological Administration in 2017, a single station cold wave is defined by a daily minimum air temperature lower than or equal to 4 °C and any one of three conditions: a decrease by no less than 8 °C within 24 h, or a decrease by no less than 10 °C within 48 h, or a decrease by no less than 12 °C within 72 h.

During a regional cooling process, a regional strong cooling event (RSCE) is recorded if the cumulative number of meteorological stations in northern China that meet the criteria of a single station cold wave is no less than 40% of the total number of stations. Because there is a time difference in the impact range of the cold air invasion path on the station temperature during the RSCE, a one-day interval is allowed in the continuous RSCE process, that is, the regional average minimum temperature is allowed to rise for only one day in this process, and then continue to decline until there is a continuous rise.

2.2.2. Morlet Wavelet Analysis

Wavelet analysis [44] is an improvement on the Fourier method and can be used to analyze time series that contain unstable energy at different frequency bands. Suppose there is a time series with equal intervals x_n and a Morlet wavelet mother function $\Psi(\eta)$ that depends on the dimensionless series parameter η. This function can be used as a wavelet function if it has 0 mean and can be determined by time and frequency. Its wavelet mother function is as follows:

$$\Psi_0(\eta) = \pi^{-1/4} e^{i\omega_0 \eta} e^{-\eta^2/2} \quad (1)$$

where ω_0 is a determined frequency, and ω_0 is taken as 6 in order to satisfy the aforementioned condition of the wavelet mother function. The Morlet wavelet is generated by Gaussian functions in the process of modulating the amplitudes of sine and cosine waves and is represented in the form of complex wavelets. When the continuous function $x_n \in L^2$, similar to the Fourier transform, the wavelet transformation result $W_n(s)$ is the convolution of the time series x_n and the scaled wavelet mother function:

$$W_n(s) = \int x_{n'} \Psi^*_{s,n} dt \tag{2}$$

$$\Psi^*_{s,n} = \frac{1}{\sqrt{s}} \Psi\left(\frac{n'-n}{s}\right) \tag{3}$$

where "*" denotes the conjugate of the complex numbers. Thus, the wavelet image—amplitude variation with scale and time—can be sketched by transforming the wavelet scale "s" and time point "n".

2.2.3. Butterworth Band-Pass Filter

The advantage of the butterworth filter [45] is that the passing frequency band can be freely selected, and the data at both ends will not be lost after filtering. In this paper, this method is used to filter the significant low frequency components of the circulation factors.

The filtering equation is as follows:

$$y(t) = a(x(t) - x(t-2)) - b_1 y(t-1) - b_2 y(t-2) \tag{4}$$

where $x(t)$ is the original sequence of the input and $y(t)$ is the filtered sequence.

The frequency response function is:

$$R_B(f) = |W(z)|^2 \tag{5}$$

where $W(z) = \frac{a(1-z^2)}{1+b_1 z+b_2 z^2}$, $z = e^{-2f\pi i\Delta}$, Δ is the sample interval.

2.2.4. Composite Analysis and Its *t*-Test

Composite analysis is an application of the significant test for the differences between two populations' means [46–48]. The *t*-test is used to test whether the mean difference is significant or not. The t-statistic is constructed as follows:

$$t = \frac{\overline{x} - \overline{y}}{\sqrt{\frac{(n_1-1){S_1}^2+(n_2-1){S_2}^2}{n_1+n_2-2}\left(\frac{1}{n_1}+\frac{1}{n_2}\right)}} \tag{6}$$

in which, $\overline{x}$ and $\overline{y}$ are the two sample means, S_1 and S_2 denote the sample standard deviation of x and y, n_1 and n_2 are the sample size of x and y, respectively. After determining the significant level α, the t-distribution table is checked according to the degrees of freedom $(n_1 + n_2 - 2)$, and if $|t| > t_\alpha$, a significant difference is considered to occur.

2.2.5. Lead-Lag Correlation Analysis

The lead-lag correlation method [48] can be used to calculate the correlation coefficients for two series of the same length, in which one of the data series is ahead or behind the other by a certain length of time. The formula is as follows:

$$r_l = \frac{\frac{1}{n-l}\sum_{t=1}^{n-l}(x_t - \overline{x})(y_{t-l} - \overline{y})}{\frac{1}{n}\sqrt{\sum_{t=1}^{n}(x_t - \overline{x})^2 \sum_{t=1}^{n}(y_t - \overline{y})^2}} \tag{7}$$

where x and y are two element time series, respectively, l is the lead or lag time, $l = 0$ denotes x and y synchronous, with $l > 0$ x leading y and $l < 0$ x lagging y. Student's t-test method is used to determine the statistical significance of the correlation coefficients.

In addition, due to the auto-correlation of the filtered data increasing, the effective degrees of freedom are calculated for the significant test of the time correlation coefficients [49–52].

3. Results

3.1. Characteristic of RSCEs in Northern China

3.1.1. Spatial and Temporal Characteristics

According to the definition of RSCEs in Section 2.2, the frequency of RSCEs in a total of 40 winters from 1980 to 2019 is shown in Table 1. It can be seen that there are 30 RSCEs in 22 winters, and the cooling process usually lasts for 3 to 5 days, with the longest duration being 9 days and the shortest being 2 days.

Table 1. Start and end dates and duration of 30 RSCEs (unit: d).

Year	Start and End	Duration	Year	Start and End	Duration
1980	2.22–2.26	5	2000	1.7–1.14	8
1982	1.4–1.8	5	2002	12.21–12.25	5
1985	12.3–12.8	6		1.25–1.29	5
1987	12.27–12.30 *	4	2005	2.13–2.17	5
	1.21–1.24	4		2.21–2.22 *	2
1988	1.7–1.14	8	2008	12.1–12.5	5
1989	1.28–1.31	4		12.16–12.22	7
	2.20–2.24	5		1.20–1.23	4
1991	12.22–12.28	7	2009	1.19–1.22	4
1992	2.5–2.9	5	2012	12.20–12.23	4
1993	1.16–1.18	3	2015	1.16–1.24	9
1995	2.13–2.20	8		2.11–2.15	5
1996	12.30–1.5	7	2018	12.2–12.8	7
1998	2.17–2.19	3	2019	12.29–12.31	3
1999	1.5–1.7	3		2.13–2.16	4

* indicates the strong cooling process with no significant low frequency period.

According to the frequency series of RSCEs in the winter of northern China from 1980 to 2019 (Figure 2a), it can be seen that there are 15 RSCEs before and after 2000, respectively, but the interannual variability after 2000 increases significantly. The variance of the frequency before and after 2000 is 0.41 and 0.93, respectively, and their difference passes the F-test at the significant level of 0.05. The variance is dependent on both frequency and amplitude of a sample data, and in Figure 2a, the much larger variance after 2000 may be greatly attributed to the amplitude of frequency of RSCEs. Based on this, a variation of approximately 20 years may be present in the amplitude and the causes of this deserve further study.

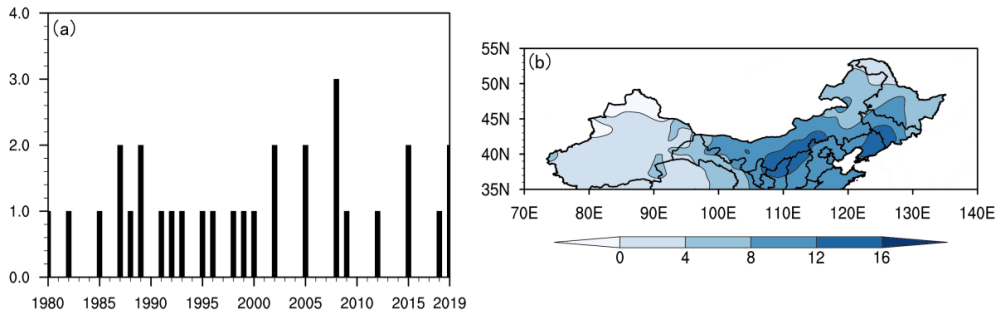

Figure 2. (**a**) Frequency of RSCEs in the winter of northern China from 1980 to 2019 (unit: number of occurrences) and (**b**) spatial distribution of cooling amplitude averaged by 30 RSCEs (unit: °C).

For each station, the difference between the minimum temperature at the start and end days of the cooling process is defined as the cooling amplitude of the station. From the distribution of cooling amplitude averaged by 30 RSCEs processes (Figure 2b), the overall cooling amplitude trend is to increase from west to east, with the large value centers ($\geq$12 °C) mainly located on the border between Inner Mongolia, Shaanxi and Shanxi, and the border area of Liaoning and Jilin. Furthermore, each RSCE has a temperature decrease of at least 8 °C, and individual events have a greater decrease, with a maximum cooling amplitude of more than 20 °C (Figure omitted).

3.1.2. Significant Low Frequency Periods

The regional average minimum temperature series are extended to both ends appropriately in 22 winters when RSCEs occurred in northern China, and Morlet wavelet analysis is used to analyze the significant low frequency periods. The significant low frequency periods of the extended minimum temperature series and the significant peaks of spectra for each year and the 22-year average are listed in Table 2.

Table 2. The significant low frequency periods of the regional average minimum temperature in northern China in 22 winters when RSCEs occurred (the periods in question pass the significant test at α = 0.1 level) and the significant peaks of each spectra.

Year	Low Frequency Periods	Peak	Year	Low Frequency Periods	Peak
1980	10–20 d; 30–60 d	0.25	1998	10–20 d	0.41
1982	10–20 d	0.28	1999	10–20 d; 20–30 d	0.36
1985	10–20 d; 20–30 d	0.28	2000	10–20 d; 20–30 d	0.39
1987	10–20 d; 20–30 d	0.40	2002	10–20 d; 20–30 d; 30–60 d	0.52
1988	10–20 d; 20–30 d; 30–60 d	0.37	2005	10–20 d	0.24
1989	10–20 d; 20–30 d	0.43	2008	10–20 d	0.38
1991	10–20 d; 20–30 d	0.30	2009	10–20 d; 20–30 d	0.34
1992	10–20 d; 20–30 d	0.20	2012	10–20 d	0.27
1993	10–20 d; 20–30 d; 30–60 d	0.39	2015	10–20 d	0.52
1995	10–20 d; 20–30 d	0.80	2018	10–20 d; 20–30 d	0.93
1996	10–20 d; 20–30 d	0.26	2019	10–20 d; 20–30 d	0.32
			22-year average	10–20 d	0.15

In Table 2, there are significant low frequency periods of 10–20 d, 20–30 d and 30–60 d for the regional average minimum temperature in northern China, among which the low frequency oscillation with a period of 10–20 d is the most significant, followed by the 20–30 d. The wavelet analysis result of the winter minimum temperature in 2015 is shown as an example in Figure 3a, with the 10–20 d period being the most significant. The low frequency oscillation with a period of 10–20 d for the 22-year average is also significant (Figure omitted). The following section focuses on the characteristics of the 10–20 d low frequency atmospheric circulation affecting RSCEs in northern China.

3.2. Association of RSCEs in Winter with Atmospheric LFO

The seasonal variation of the atmospheric elements was first removed, and then the 10–20 d low frequency component was extracted by filtering. Each complete cycle of the low frequency variation of temperature is divided into 8 phases. Phase 3 is the peak, i.e., the phase when the cooling starts. Phase 7 is the valley, i.e., the phase when the temperature drops to a minimum. Phases 4–6 are the falling phases, and phases 8–2 are the rising phases. The minimum temperature drops from the peak to the valley, which can correspond to an RSCE. Therefore, the analysis focuses on phases 3, 5, and 7. According to each RSCE and the 10–20 d low frequency component of the regional average minimum temperature in winter (similar to Figure 3b), the low frequency circulation fields of the specific days corresponding to the 3rd (peak), 5th (transition), and 7th (valley) phases for the 28 RSCEs

are studied by composite analysis, so as to reveal the key low frequency circulation systems and their evolution characteristics that cause RSCEs in northern China.

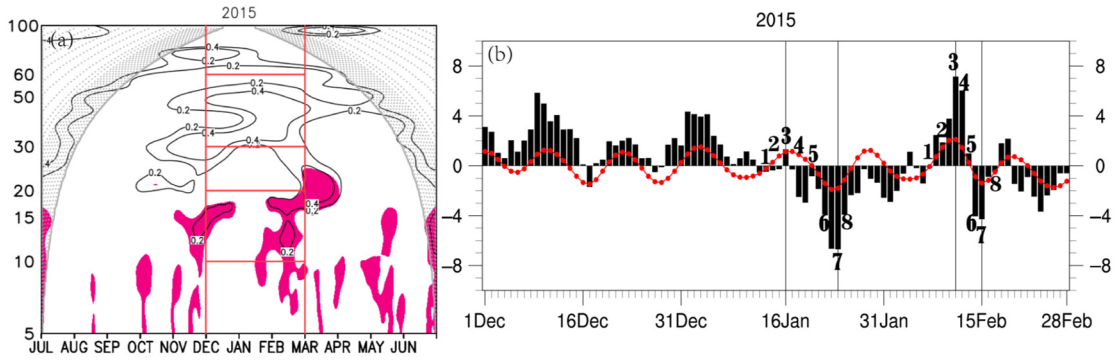

Figure 3. (**a**) Wavelet analysis of the regional average minimum temperature series in northern China in 2015. The area between the vertical red lines represents the period from December to February (the shaded contour encloses regions of larger than 0.1 significance), and the horizontal red lines correspond to 10, 20, 30, and 60 d, respectively. (**b**) Minimum temperature departure series (bar) and its 10–20 d component (curve). The interval between the two vertical lines denotes the strong cooling process (unit: °C).

3.2.1. Characteristics of Low Frequency Circulation in the Middle and Lower Troposphere

The phase evolution characteristics of the low frequency circulation systems are firstly analyzed in the mid-low troposphere (Figure 4). The changes in 850 hPa temperature are in good agreement with that of the surface temperature when the radiation effect is not considered [53], so the characteristics of the surface temperature are approximately reflected by analyzing the 850 hPa temperature.

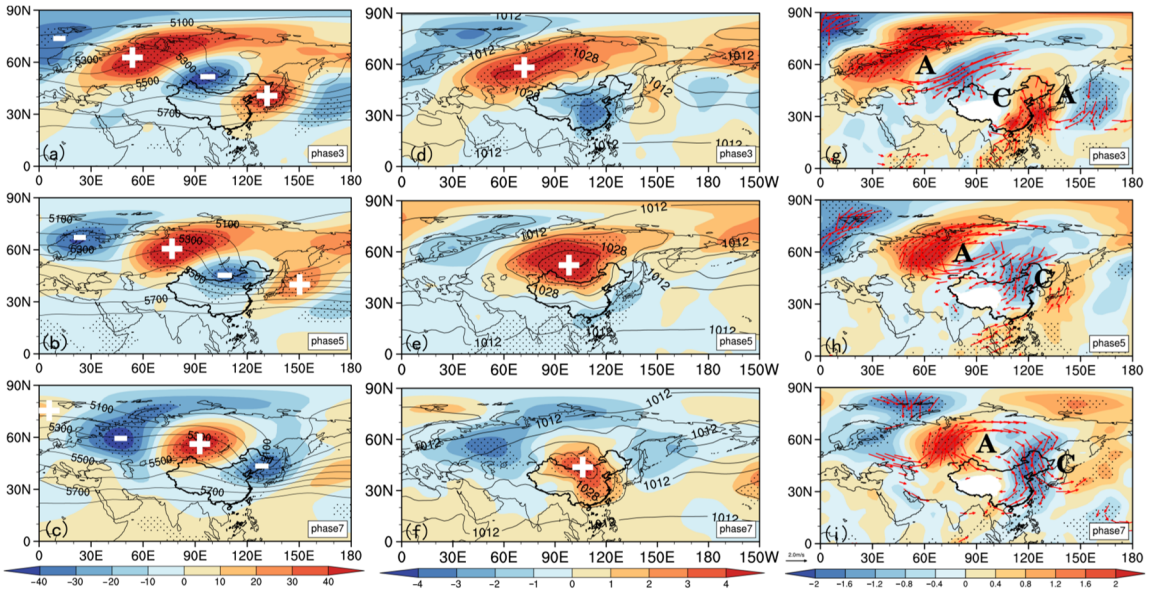

Figure 4. (**a**–**c**) 500 hPa geopotential height (unit: gpm), (**d**–**f**) SLP (unit: hPa) and (**g**–**i**) 850 hPa wind (vector, unit: m/s, the blank area is the Tibetan Plateau) and temperature (shaded, unit: K) measured in 28 RSCEs at phase 3, 5, and 7, respectively. (Shaded area: 10–20 d component; contour: unfiltered data; dotted area and red vector enclose regions of larger than 0.01 significance).

As is shown in Figure 4, the phase evolution of the low frequency circulation in the mid-low troposphere takes on a quasi-barotropic structure. At phase 3 (Figure 4a), there is a "−", "+", "−", "+" low frequency teleconnection wave train over the Eurasian

mid-high latitude in the 500 hPa geopotential height field. The high pressure ridge in the Urals is relatively strong. The area around Lake Ba-Bei is controlled by a low pressure trough. There is a large area of low frequency positive anomaly from the Caspian Sea to the northeast of Lake Baikal in the sea level pressure (SLP) field (Figure 4d), and the center is located in the Western Siberian Plain, indicating the SH is strong and northwestwardly located. Moreover, there are corresponding low frequency cyclones and anticyclones in the 850 hPa wind field (Figure 4g). The northerly air flow in front of the high ridge of the Urals (Figure 4a) guides the low-level cold air from the west-middle of Central Siberia to west Siberia to eastern Lake Balkhash into Xinjiang, making Xinjiang begin to cool down. However, Xinjiang and Qianghai are influenced by the periphery of the cold center, resulting in weaker cooling here.

During phases 3–7, the aforementioned Eurasian low frequency teleconnection wave train gradually moves to the southeast. At phase 5, the low frequency high pressure ridge and low pressure trough in the 500 hPa geopotential height (Figure 4b) move to the northwest and southeast of Lake Ba-Bei, respectively. The SH in the SLP field (Figure 4e) also moves southeast and extends to northern China, with the center located near Lake Ba-Bei. In the 850 hPa wind (Figure 4h), the cold advection is led by the northerly airflow in front of the mid-level ridge to the central and eastern regions of northern China from Central Siberia via Lake Baikal and its eastern region, resulting in significant cooling there, especially in the central region (Figure 4e).

At phase 7, there is a "+", "−", "+", "−" low frequency teleconnection wave train in the Eurasian mid-high latitude at the 500 hPa geopotential height (Figure 4c). The meridional circulation is obviously increased. The Lake Ba-Bei high ridge is stronger, and the East Asian trough is westward and deeper. In the SLP (Figure 4f), the low frequency positive anomaly controls the region from the southeast of Lake Ba-Bei to the southeast coast of China, making the SH strong and southeastward. The northerly airflow in front of the Lake Ba-Bei high ridge leads to cold advection from the east of Central Siberia into Northeast China including in its south, causing significant cooling on the ground (Figure 4i). Because of the lasting impact of cold air from the mid-high latitude, the average temperature in northern China drops to the lowest at this time.

In summary, as the mid-level low frequency circulation systems move from northwest to southeast during the cooling process, the low-level cold air gradually affects northern China from west to east, resulting in large-scale RSCEs. The phase of the low frequency circulation system affecting the west and east of northern China is the opposite, and the meridional circulation affecting the east is also stronger.

3.2.2. Characteristics of Low Frequency Jets

When the cold wave breaks out, the interaction between upper waves and jets causes a conversion of energy and momentum, which will lead to a change in the intensity of the East Asian upper level jets [54,55] and then affect the intensity and path of cold air at high latitude. Therefore, it is of great significance to research the relationship between the changes in the upper jet stream and cold air activity.

In the low frequency 300 hPa zonal wind field (Figure 5), there is a low frequency strong zonal wind negative anomaly in Central Siberia at phase 3 (Figure 5a), that is, the upper temperate jet is weak, which is favorable for cold air to move southward from the middle and west of Central Siberia. The region from Xinjiang to Northeast China is a belt-like distribution of positive low frequency zonal wind anomalies, indicating that the subtropical westerly jet is strong here. This is conducive to the accumulation of cold air in Xinjiang, causing the beginning of a cooling down in the west of northern China. As time goes on, the above-mentioned negative and positive low frequency zonal wind anomalies move southeast. At phase 5 (Figure 5b), the negative (positive) anomaly shifts to the vicinity of Lake Ba-Bei (from the middle of northern China to the Japanese Islands), making the temperate jet weaker and the subtropical jet stronger. At phase 7 (Figure 5c), the negative (positive) anomaly of low frequency zonal winds moves to the south of Lake Ba-

Bei—northern China (the Yellow Sea—the southern Japan archipelago), which is favorable for cold air to invade and gather in the east of northern China, causing the occurrence of RSCEs.

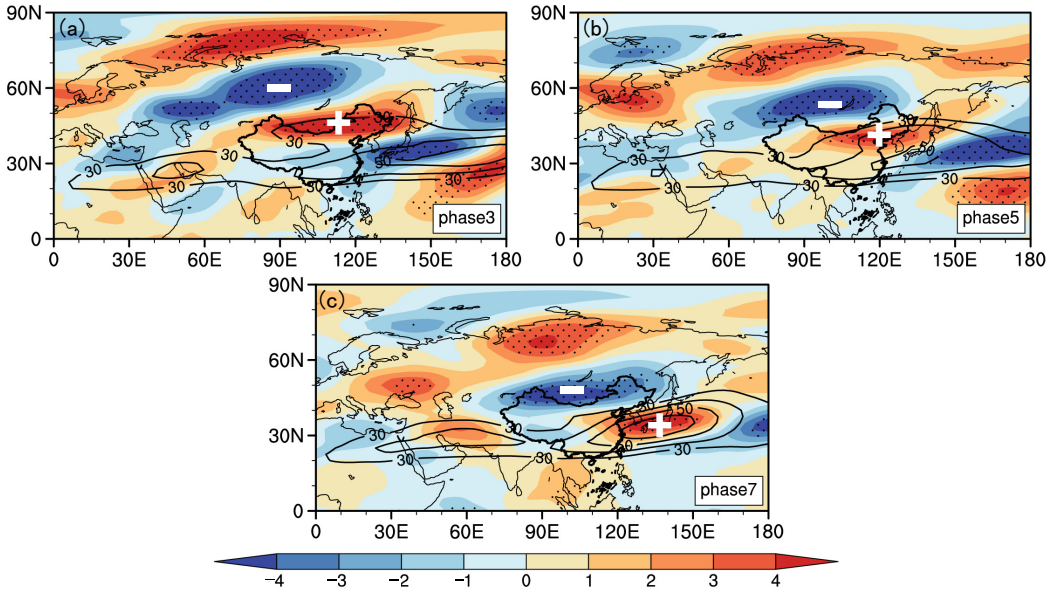

Figure 5. Low frequency 300 hPa zonal wind (shaded: 10–20 d component, dotted area encloses regions of larger than 0.01 significance; contour: westerly jet, unit: m/s) at phase 3 (**a**), 5 (**b**), and 7 (**c**), respectively.

To sum up, the upper level jets in the upper troposphere that are weaker in the north and stronger in the south gradually move from the northwest to the southeast in the whole process of RSCEs, which allows cold air to go southward and accumulate in the corresponding areas, causing RSCEs to occur under the continuous influence of strong cold air.

3.3. Characteristics of Low Frequency PV

3.3.1. Characteristics of Low Frequency PV Anomalies in the Tropopause

Potential vorticity (PV) can be considered as the optimal indicator to characterize cold air [56,57]. In winter, the isentropic potential vorticity (IPV) is conserved for a long time in the adiabatic and frictionless atmosphere, so the cold air characteristics of RSCEs can be traced based on its conservation. Both the mid-high latitude tropopause and the lower stratosphere have high PV centers [58,59]. The 315 K isentropic surface that coincides with the tropopause in the polar frontal region is generally used for IPV analysis in winter in the northern hemisphere [58–60]. On this surface, the 2 PVU line can represent the dynamic tropopause, and the 4 PVU line represents the activity range of strong cold air in the upper stratosphere [61–63]. It has been established that the dynamic tropopause is the conversion layer between the stratosphere and troposphere, and its descent indicates the intrusion of high PV cold air [64–67]. The evolution characteristics of the low frequency IPV on the 315 K isentropic surface are analyzed as follows (Figure 6).

In Figure 6, at the beginning of the cooling down (Phase 3, Figure 6a), the low frequency negative PV anomaly near the Urals and the Sea of Japan in the stratosphere causes the 4 PVU line to lift northward. The southern part of the low frequency positive PV center between Lake Ba-Bei in the stratosphere covers the northern province of Xinjiang in China. The positive anomaly of the low frequency PV makes the 4 PVU and 2 PVU lines move southward, and the cyclonic circulation maintains the high PV center here.

At phase 5 (Figure 6b), the above low frequency positive and negative PV anomaly centers move southeastward, and such a blockage situation maintains the southward movement of strong cold air from the high PV within the 4 PVU line in the upper stratosphere.

The connection of the positive PV anomaly in the polar region and in the mid-high latitude further strengthens the high PV cold air accumulated at the bottom of the stratosphere. The low frequency positive PV center shifts to the area between the south of Lake Baikal and northern China, encompassing the central part of the north. The 2 PVU line shifts further southward than in phase 3, and the positive PV cold air invades the central part of northern China significantly.

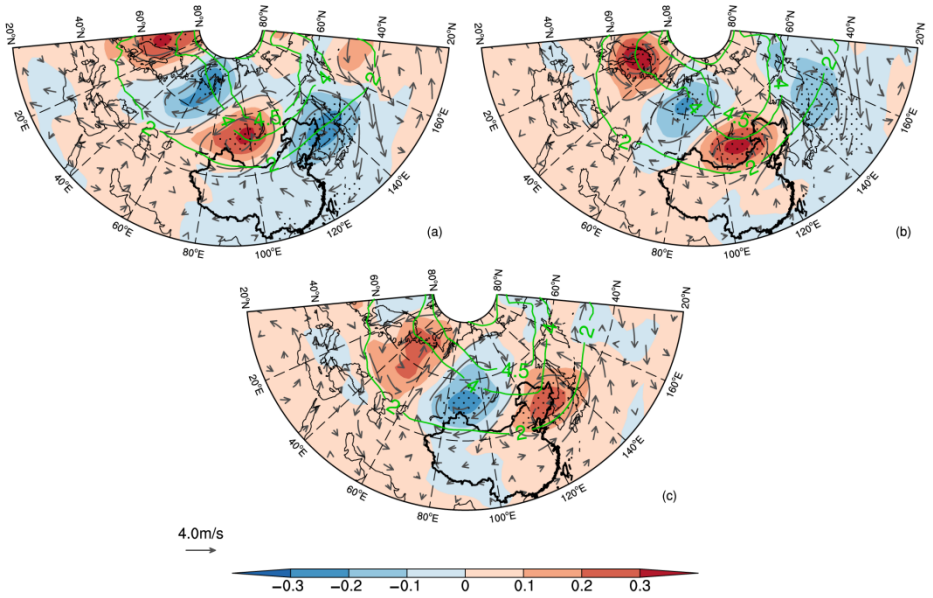

Figure 6. The IPV (contour, unit: PVU, 1 PVU = 10^{-6} $m^2 \cdot K \cdot s^{-1} \cdot kg^{-1}$) and 10–20 d low frequency IPV (shaded, unit: PVU, dotted area encloses regions of larger than 0.01 significance) on the 315 K isentropic surface at phase 3 (**a**), 5 (**b**), and 7 (**c**), respectively.

At phase 7 (Figure 6c), the center of the low frequency high PV center moves to the junction area between Northeast China and the Sea of Japan. The strong cold air in the upper and lower stratosphere also moves eastward here. The 2 PVU line in the northeast extends southward to the Shandong Peninsula of China, and the impact of the positive PV center in the tropopause over northern China is strongest.

In summary, the cyclonic circulation always maintains the high PV center in the lower stratosphere during the whole cooling process in northern China. Furthermore, the high PV center moves eastward and southward via the north of Lake Ba-Bei, southern Lake Baikal and the northeast to the Sea of Japan, causing the 2 PVU line to move south significantly. The cold air gradually invades northern China from west to east.

3.3.2. Characteristics of the Downward Propagation of Low Frequency PV Anomaly in the Upper Level of the Troposphere

The high PV cold air has very strong static stability. While moving southeast, it will be incompatible with the surrounding temperature and pressure field, resulting in the abnormal downward propagation of the high PV and the vertical extension of the strong cold air [53,58,59]. In order to further understand the vertical extension and change of cold air in the tropopause during the cooling process in northern China, and to explore the reasons for the intensity change of the cold air in the lower layer, combined with the movement path of the key low frequency circulation systems in Section 3.3.1, the latitude–pressure evolution of the averaged low frequency PV along latitudes 80–90° E, 100–110° E, and 120–130° E is given at phases 3, 5 and 7, respectively (Figure 7).

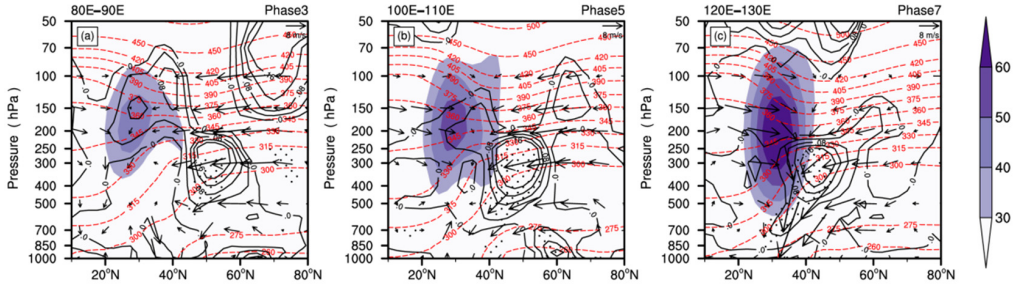

Figure 7. Latitude–pressure profiles of zonally averaged westerly jet (shaded, unit: m/s), potential temperature (red dashed line, unit: K), wind (vectors, unit: m/s), and 10–20 d low frequency isobaric PV (contour, unit: PVU, dotted area encloses regions of larger than 0.01 significance) at phases 3, 5 and 7 along latitudes 80–90° E (**a**), 100–110° E (**b**), and 120–130° E (**c**), respectively.

As can be seen from Figure 7 that the anomalous center of the 10–20 d low frequency high PV column in the upper level is located near 300–400 hPa over northern Xinjiang (50° N) at phase 3 (Figure 7a), and the ground center is located in the Western Siberian Plain north of 60° N, and that both are controlled by northerly wind. The westerly jet on the south side of the high-level PV column is strong in the upper and weak in the lower levels, which is conducive to the accumulation of high-level cold air at 300–400 hPa and the advection southward along the isentropic surface, eventually leading to the beginning of cooling down in Xinjiang.

At phase 5 (Figure 7b), the low frequency high PV column extends southward and downward, and the inclination of the isentropic surface near its center (400 hPa) increases. The westerly jet is further strengthened and extended downward. The vertical circulation near the center of high PV is reinforced, and a large amount of cold air is transported southward and downward along 300–315 K isentropic surfaces to the central region in northern China, causing cooling down there. In addition, the high PV center at high latitudes on the ground moves slightly southward, favoring cooling down in the middle of northern China.

The westerly jet near the center of the low frequency high PV column (40° N) continues to strengthen and expand downward, and its range has dropped to around 500 hPa at phase 7 (Figure 7c). The vertical circulation near the high PV column is further enhanced, strongly guiding the cold air at the mid-upper level downward to the ground in the east of northern China, resulting in the development of persistent cooling from the west to the east of northern China.

In conclusion, during the whole process of strong cooling, the high PV cold air column near 300–400 hPa in the upper troposphere first affects Xinjiang and then gradually affects the middle and northeast of China, and there is a combination of gradually increasing upper level jets and vertical meridional circulation, so that the cold air of the high PV continues to propagate downward to the lower latitudes and levels along the 300–315 K isentropic surfaces, resulting in a large-scale strong cooling event in northern China.

3.4. Dynamic Characteristics of Low Frequency Circulation Vertical Structure

The tilted isentropic surface is not only the path of cold air intrusion in the upper layers but also the region where vertical vorticity is most likely to develop [56]. According to the theory of conservation of PV, the rotation of the strong cold air will be strengthened when the high PV column is stretched in the vertical direction, that is, the positive vorticity will increase, and it is the opposite for the low PV center. To investigate the dynamical evolution characteristics of the vertical structure of the low frequency circulation, height-longitude vertical profiles of the low frequency vorticity and divergence (Figure 8) along the latitudes 45–55° N, 40–50° N and 35–45° N are made according to the latitudes of the anomalous centers of the key systems at phases 3, 5, and 7 shown in Figures 4, 6 and 7.

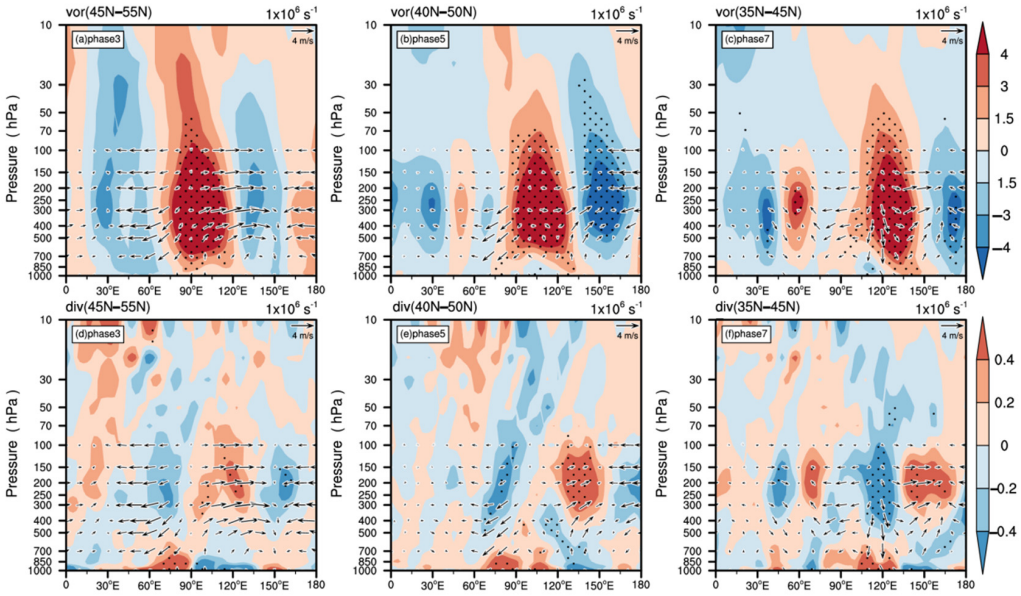

Figure 8. (**a**–**c**) Height–longitude profiles of meridional average 10–20 d low frequency vorticity, and (**d**–**f**) divergence along the latitudes 45–55° N, 40–50° N, and 35–45° N at phases 3, 5, and 7, respectively (shaded, unit: 10^{-5} s^{-1}, dotted area encloses regions of larger than 0.01 significance) and 10–20 d low frequency wind (vector, unit: m/s).

As seen in Figure 8, the stratosphere and troposphere in the north of Xinjiang are controlled by low frequency positive vorticity at phase 3 (Figure 8a), indicating that the trough at Lake Ba-Bei is deep, causing the upper level cold air to affect Xinjiang. The stream field in the eastern side of the key area (75–105° E) diverges (positive anomaly) in the middle and upper troposphere and converges (negative anomaly) in the lower troposphere (Figure 8d), resulting in the anomalous ascending motion being strengthened and the trough at Lake Ba-Bei deepening. The stream field in the middle and upper troposphere converges and diverges in the lower troposphere on the western side of the key area (75–105° E) (Figure 8d), leading to the anomalous downward movement strengthening, which can develop the SH. The cold air on the ground begins to invade Xinjiang.

At phase 5 (Figure 8b), as the low frequency high PV cold air in the upper level gradually propagates downward during the process of eastward and southward movement (Figure 7b), the low frequency positive vorticity in the stratosphere and troposphere significantly intensifies. The eastward movement of cyclonic vorticity in turn leads to the eastward shift and enhancement of the trough in the south of Lake Baikal. The cold air guided by the northerly airflow behind the trough leads to cooling in the middle of northern China. At this time, the convergence in the middle and upper troposphere and divergence in the lower layer (Figure 8e) on the western side of the key area (90–120° E) and to its west have enhanced the descending motion, causing the maintenance and eastward movement of the SH.

At phase 7 (Figure 8c), with the continuous downward propagation of the high PV cold air at the upper level gradually moving eastward, the low frequency positive vorticity within the stratosphere and troposphere keeps intensifying and moving eastward, making the East Asian trough deeper. There is convergence in the lower troposphere and divergence in the middle and upper layers near 135–150° E, accompanied by strong ascending motion, which is conducive to the maintenance of the deep East Asian trough and AL. Around 105–135° E, there is convergence in the upper troposphere and divergence in the lower troposphere (Figure 8f), accompanied by strong descending motion, which is favorable for the SH to strengthen and move southward. The cold air arrives in the northeast of China, with the cooling reaching its strongest.

All in all, during the whole cooling process, as the high-level PV cold air gradually moves eastward and propagates downward, the low frequency positive vorticity in the stratosphere and troposphere keep moving and enhancing, making the trough deepen and move eastward. Meanwhile, the convergence in the upper troposphere, the divergence in the lower layer, and the strong descending motion behind the trough make the SH strengthen and move consistently southeastward, and the cold air affects the entire northern China in turn.

3.5. Low Frequency Prediction Signals

It has been found that persistence of temperature fluctuations exhibits long-term memory with scaling behavior [68,69]. Therefore, the increase in the frequency, intensity, and duration of extreme temperature events due to climate change will be more pronounced than expected. For much of the world, information on seasonality and medium-term forecasts can help to anticipate extreme events with enough time to take action [70,71].

The low frequency characteristics of atmospheric circulation and cold air in the stratosphere and troposphere during the process of the RSCEs are analyzed in the previous section. On this basis, low frequency prediction signals for RSCEs are sought in order to provide some reference for the extended range forecast of RSCEs in the winter of northern China. The 10–20 d regional averaged minimum temperature series for 28 processes are connected into a new series in northern China, and its lead–lag correlation coefficients with the 10–20 d 500 hPa geopotential height field are calculated (Figure 9). Negative numbers indicate the number of days that the low frequency geopotential height field leads the minimum temperature series. Negative (positive) correlation regions correspond to positive (negative) anomalies in the height field.

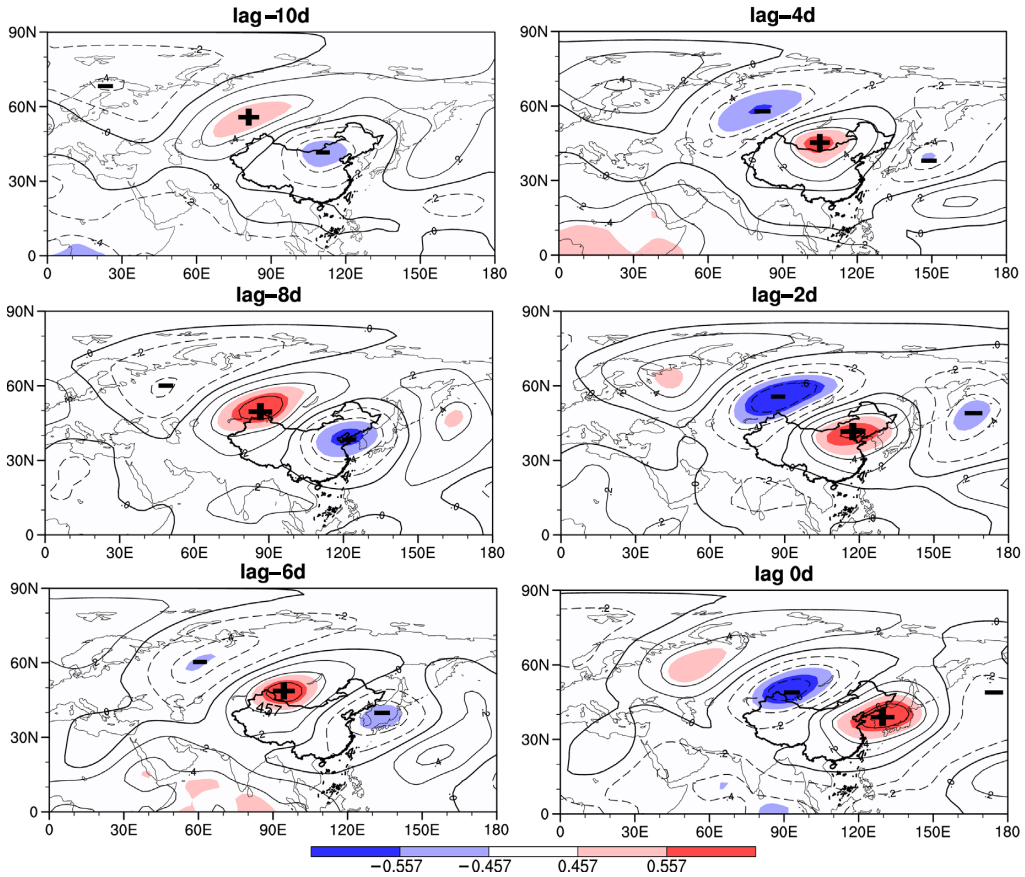

Figure 9. Distribution of lead–lag correlation coefficients between the 10–20 d regional average minimum temperature series in northern China and the 500 hPa geopotential height fields. Shaded areas enclose regions of larger than 0.1 significance.

In Figure 9, there is a significant low frequency teleconnection wave train of "−", "+", "−" from the East European Plain and West Siberian Plain to East Asia at −10 d, and there is a low frequency "+", "−", "+" abnormal wave train in the corresponding 500 hPa geopotential height field. The significant correlation wave train continues to move eastward and southward and strengthens. At −8 d, the Urals area is covered by negative correlation, and the Lake Ba-Bei area is controlled by significant positive correlation, which means the Ural blocking high is enhanced and the Lake Ba-Bei is controlled by an anomalous trough. The cold air at high latitude reaches Xinjiang in China along the northerly airflow in front of the Urals ridge, making Xinjiang begin to cool down. From −6 d to −4 d, the above wave train continues to move eastward and southward, and the influence range of cold air gradually expands eastward. This is similar to the evolution from phase 3 (Figure 4a) to phase 5 (Figure 4b) in the corresponding 500 hPa geopotential height field. At −4 d, the significant negative and positive correlation zones lie in the northwest and southeast of Lake Ba-Bei, respectively, corresponding to the low frequency ridge and trough of the 500 hPa geopotential height field (similar to Figure 4b). The cold air at high latitude, guided by the northerly airflow in front of the low frequency ridge, affects the middle of northern China. At −2 d, as the significant correlation areas continue to move eastward and southward, the cold air has a lasting effect on the center and east of northern region. At 0 d, the Lake Ba-Bei (Northeast China and coastal areas) is governed by a significantly negative (positive) correlation. In the corresponding 500 hPa geopotential height field (similar to Figure 4c), the low frequency blocking high in Lake Ba-Bei is strong and the East Asian trough is deep, so the cold air has an impact on the northeast of China, eventually causing the occurrence of RSCEs.

Thus, special attention should be paid to the positive (negative) low frequency height anomalies in the East European Plain (in the West Siberian Plain) at −10 d for RSCEs in northern China. At −8, −4, and 0 d, the ridges and troughs caused by the movement of these low frequency positive and negative anomalies will gradually cause cooling from west to east, eventually leading to the occurrence of RSCEs in the whole northern region.

4. Discussion

The influence of atmospheric low frequency oscillations with a period of 10–20 d on the regional strong cooling events (RSCEs) in the winter of northern China is investigated. The key atmospheric low frequency systems and the interaction process of the cold air between the stratosphere and troposphere are disclosed, and the extended-range forecast signals for RSCEs have been extracted.

In general, the interannual variability in the frequency of RSCEs is increasing. The overall cooling amplitude of the RSCEs tends to increase from west to east, with the large value centers mainly located on the border among Inner Mongolia, Shaanxi, and Shanxi and on the border between Liaoning and Jilin. The 10–20, 20–30 and 30–60 d low frequency periods are significant for the regional average minimum temperature series in northern China, especially the low frequency oscillation with a period of 10–20 d.

The key low frequency systems, cold air paths, and sources that affect RSCEs in northern China are given. During the cooling process, the upper level low frequency circulation systems move from northwest to southeast consistently, which guides the lower-level cold air to gradually invade the entire region from west to east. The phases of the low frequency circulation systems affecting the RSCEs in the west and east of the northern region are the opposite, and the low frequency meridional circulation affecting the east is stronger. The key low frequency systems affecting the RSCEs in the west, middle, and east of the northern region are the Ural blocking high and the Lake Ba-Bei trough, the blocking high in the northwest and low trough in the southeast of Lake Ba-Bei, the Lake Ba-Bei blocking high and the East Asia trough, respectively, and the SH extending and moving southeastward with the blocking high all the time. The low frequency upper-level jets are weaker in the north and stronger in the south, which is conducive to cold air moving

southward. Therefore, the region around Lake Baikal, where cold air passes through, is the key area that affects RSCEs in northern China.

The low frequency high PV center in the lower stratosphere moves southeastward along the 315 K isentropic surface via the north of Lake Ba-Bei, southern Lake Baikal and Northeast China to the Sea of Japan, causing the 2 PVU line to move significantly southward. The high PV column at mid-high latitude in the middle and high troposphere extends vertically and moves southeastward. Meanwhile, under the influence of the gradually enhanced upper level westerly jets and vertical meridional circulation, it continues to propagate downward to the mid-low level at lower latitude along the 300–315 K isentropic surfaces, resulting in the low frequency positive vorticity enhancing and the key trough deepening and moving eastward. Moreover, the convergence in the upper troposphere, the divergence in the lower layer, and the descending motion behind the trough are enhanced, which also makes the SH strengthen and move southward. During the whole cooling process, the systems at the high and low levels cooperate with each other, and direct cold air from the mid-upper level into northern China. Significantly, the intensity of PV cold air descending from the stratosphere into the troposphere is relatively weaker, and PV cold air rarely descends directly to the ground. Its descent mainly affects the strength and movement of key systems in the mid-upper the troposphere through dynamic processes. Therefore, the cold air that triggers RSCEs still mainly comes from the high-latitude and polar regions in the troposphere and invades northern China through the atmospheric circulation.

In the early stages of RSCEs in northern China, low frequency positive and negative anomalies at 500 hPa geopotential height field in the Eastern European Plain and West Siberian Plain at −10 days need to be paid attention to, as they are the prediction signals of the key low frequency ridges and troughs.

5. Conclusions

In recent years, issues about the relationship between stratospheric ozone depletion in the northern hemisphere and climate change have received widespread attention. The 2010–2011 winter record-breaking ozone loss was triggered by the extremely low stratospheric temperatures that are linked to climate change [72–74]. The extreme cooling of the stratospheric temperature can exacerbate stratospheric ozone depletion and vice versa [72,75]. It is claimed that the occurrence of ozone depletion events leads to a decrease in the internal temperature of the polar vortex in the stratosphere, thus making the Arctic polar vortex and the polar night jet stronger [75,76].

When the disturbance of the stratospheric polar vortex caused by stratospheric sudden warming (SSW) occurs, the high IPV anomaly signal (i.e., cold air within the stratosphere) splitting from the polar vortex will move eastward and southward toward Eurasia, which can affect the circulation systems in the troposphere through dynamical processes (similar to those in Section 3.3) and eventually lead to a strong cooling in China [77]. On the other hand, it has been observed that the strengthening of the polar night jet can weaken the activity of the Rossby wave at mid-high latitude in the troposphere, making the westerly jets accelerate [78,79]. In addition, the westerly jets are very important for cold air activity (similar to those in Section 3.2).

According to the above study, we infer that when the anomaly (such as SSW) occurs in the stratosphere, the enhancement of the Arctic polar vortex and the polar night jet caused by the stratospheric ozone depletion in the northern hemisphere may impact the circulation systems in the troposphere through dynamical processes and finally lead to RSCEs in northern China. However, the specific interactions between stratospheric ozone depletion in the northern hemisphere and RSCEs still deserve further scientific study.

In addition, the low frequency effects of the external forcing factors on RSCEs have not been explored. The variations of RSCEs interannual variability around the year 2000 have not been discussed in detail. These two issues are also worthy of further study.

Author Contributions: Formal analysis, W.Z. and L.L.; writing—original draft preparation, W.Z. and L.L.; writing—review and editing, W.Z., L.L. and J.R. All authors have read and agreed to the published version of the manuscript.

Funding: This research was funded by the National Key Research and Development Program of China (2018YFC1505602).

Data Availability Statement: All datasets presented in this study are included in the article.

Acknowledgments: The authors appreciate all anonymous reviewers for their helpful comments and suggestions.

Conflicts of Interest: The authors declare no conflict of interest.

References

1. IPCC. Climate Change 2021: The Physical Science Basis. 2011. Available online: https://www.ipcc.ch/report/ar6/wg1/downloads/report/IPCC_AR6_WGI_Full_Report.pdf (accessed on 6 August 2021).
2. Wang, Z.Y.; Ding, Y.H. Climate Change of the Cold Wave Frequency of China in the Last 53 Years and the Possible Reasons. *Chin. J. Atmos. Sci.* **2006**, *30*, 1068–1076. [CrossRef]
3. Ding, Y.H.; Li, Q.P.; Liu, Y.J.; Zhang, L.; Song, Y.F.; Zhang, J. Atmospheric Aerosols, Air Pollution and Climate Change. *Meteorol. Mon.* **2009**, *35*, 3–14. [CrossRef]
4. Huang, H.Q.; Han, X. Variation trend analysis of the cold airs in the East Asian. *Mar. Forecast.* **2014**, *31*, 69–75. [CrossRef]
5. Zhou, L.; Sun, Z.B. Activity characteristics of cold air in China from 1961 to 2010. *Trans. Atmos. Sci.* **2015**, *38*, 342–353. (In Chinese) [CrossRef]
6. Li, L.P.; Ni, W.J.; Li, Y.G.; Guo, D.; Gao, H. Impacts of Sea Surface Temperature and Atmospheric Teleconnection Patterns in the Northern Mid-Latitudes on Winter Extremely Cold Events in North China. *Adv. Meteorol.* **2021**, *2021*, 1–15. [CrossRef]
7. Zhu, W.L.; Lin, Q.Q.; Wang, Z.Z.; Shen, X.Y. Climatological variability of cold air processes over China in recent 60 years. *Meteorol. Mon.* **2022**, *48*, 1–13. [CrossRef]
8. Yang, Q.M. Study of the method of the extended-range forecast for the low frequency rainfall over the lower reaches of the Yangtze River in summer based on the 20–30 day oscillation. *Acta Meteorol. Sin.* **2014**, *3*, 494–507. [CrossRef]
9. Li, X.; Wang, S.G.; Shang, K.G.; Zhou, H.; Li, Y. Extended range weather forecasting based on lunar-solar calendar superposition. *J. Lanzhou Univ. Nat. Sci.* **2015**, *51*, 526–530. [CrossRef]
10. Ding, Y.H. *Advanced Synoptic Meteorology*; China Meteorological Press: Beijing, China, 1991; pp. 328–330. (In Chinese)
11. Zhu, Q.G.; Lin, J.R.; Shou, S.W.; Tang, D.S. *Principles and Methods of Synoptic Meteorology*; China Meteorological Press: Beijing, China, 1992; pp. 377–418.
12. Miao, Q.; Gong, Y.F.; Bai, Z.B. Characteristics of low frequency oscillations during cold waves in winter 2011/2012 and its coupling with the low frequency system at 500 hPa. *Trans. Atmos. Sci.* **2016**, *39*, 608–619. (In Chinese) [CrossRef]
13. Ma, X.Q.; Ding, Y.H.; Xu, H.M.; He, J.H. The Relation between Strong Cold Waves and Low frequency Waves During the Winter of 2004/2005. *Chin. J. Atmos. Sci.* **2008**, *32*, 380–394. [CrossRef]
14. Sun, C.H.; Ren, F.M.; Zhou, B.; Gong, Z.Q.; Zuo, J.Q.; Guo, Y.J. Features and possible causes for the low temperature in winter 2011/2012. *Meteorol. Mon.* **2012**, *38*, 884–889. [CrossRef]
15. Guo, G.F.; Zhou, Y.H.; Gao, Z.X.; Du, L.M. Exploration of possible causes for the low temperature throughout the winter of 2011 in Yangtze River basin. *Torrential Rain Disasters* **2013**, *32*, 176–181. [CrossRef]
16. Shen, H.Y.; Ding, Y.G.; Zhang, J. Inter-decadal variations of winter air temperature in north China and its circulation background. *Sci. Meteorol. Sin.* **2010**, *30*, 338–343. [CrossRef]
17. Zhu, H.X.; Chen, W.; Feng, T. Interannual variations of Siberian High during boreal winter and its influence on East Asian temperature. *Plateau Meteorol.* **2019**, *38*, 685–692. [CrossRef]
18. Gong, D.Y.; Zhu, J.H.; Wang, S.W. The Influence of Siberian High on Large-scale Climate over Continental Asia. *Plateau Meteorol.* **2002**, *21*, 8–14. [CrossRef]
19. Lan, L.R.; Li, D.L. Interannual and interdecadal anomaly features of Siberian High and their impact on winter temperature of China. *Plateau Meteorol.* **2016**, *35*, 662–674. [CrossRef]
20. Yao, H.R.; Li, D.L. The relationship between Asian jets and the winter monsoon and their impact on climate in China. *Acta Meteorol. Sin.* **2013**, *71*, 429–439. [CrossRef]
21. Zhang, C.Y.; Zhang, Y.C. The characteristics of East Asian jet stream in severe snow storm and freezing rain processes over southern China in early 2008. *J. Trop. Meteorol.* **2013**, *29*, 306–314. [CrossRef]
22. Ye, D.; Zhang, Y.C. Association of concurrent variation between the East Asian polar front and subtropical jets with winter cold air activity in China. *Chin. J. Atmos. Sci.* **2014**, *38*, 146–158. (In Chinese) [CrossRef]
23. Ding, Y.H.; Liang, P. Extended Range Forecast Basing on MJO. *Meteorol. Mon.* **2010**, *36*, 111–122. [CrossRef]
24. Li, C.Y. *Atmospheric Low Frequency Oscillations*; China Meteorological Press: Beijing, China, 1993.
25. Matthews, A.J.; Hoskins, B.J.; Masutani, M. The global response to tropical heating in the Madden-Julian Oscillation during Northern winter. *Q. J. R. Meteorol. Soc.* **2004**, *130*, 1991–2011. [CrossRef]

26. Zhu, Y.J.; Jiang, J. The intraseasonal characteristics of wintertime persistent cold anomaly in China and the role of low frequency oscillation in the low latitude and midlatitude. *J. Trop. Meteorol.* **2013**, *29*, 649–655. [CrossRef]
27. Zhang, W.; Jiang, J. Influence of Madden-Julian Oscillation on winter persistent cold events in China. *J. Meteorol. Sci.* **2015**, *35*, 422–429. [CrossRef]
28. Murakami, T. Winter Monsoonal surges over East and Southeast Asia. *J. Meteorol. Soc. Japan. Ser. II* **1979**, *57*, 133–158. [CrossRef]
29. Jin, Z.H.; Sun, S.Q. The characteristics of low frequency oscillations in winter monsoon over the eastern Asia. *Sci. Atmos. Sin.* **1996**, *20*, 101–111. [CrossRef]
30. Qi, D.M.; Li, Y.Q.; Chen, Y.R.; De, Q. Submonthly timescales oscillation characteristics of the east Asian winter monsoon and its effect on the temperature in southwest China-a case study in 2010. *J. Trop. Meteorol.* **2016**, *32*, 19–30. [CrossRef]
31. Yang, S.; Zhu, Q.G. Oscillation and its Relation to Cold air Activities in Asian Winter. *J. Nanjing Inst. Meteorol.* **1990**, *13*, 339–347. [CrossRef]
32. Ma, N.; He, L.Y.; Liang, S.J.; Guo, J. Low frequency characteristics of winter-time cold air activity in the Beijing-Tianjin-Hebei region and the impacts of low frequency variation of the Siberian High. *Acta Geogr. Sin.* **2020**, *75*, 485–496. [CrossRef]
33. Ding, Y.H. The propagation of the winter monsoon during clod air outbreaks in east Asia and the associated planetary-scale effect. *J. Appl. Meteorol. Sci.* **1991**, *2*, 124–132.
34. Suo, M.Q.; Ding, Y.H.; Wang, Z.Y. Relationship between Rossby wave propagation in southern branch of westerlies and the formation of the southern branch trough in wintertime. *J. Appl. Meteorol. Sci.* **2008**, *19*, 731–740. [CrossRef]
35. Yang, Q.M. Extended-Range Forecast for the Low frequency Oscillation of Temperature and Low-Temperature Weather over the Lower Reaches of the Yangtze River in Winter. *Chin. J. Atmos. Sci.* **2021**, *45*, 21–36. (In Chinese) [CrossRef]
36. Kim, B.M.; Lim, G.H.; Kim, K.Y. A new look at the midlatitude MJO teleconnection in the Northern Hemisphere winter. *Q. J. R. Meteorol. Soc.* **2016**, *132*, 485–503. [CrossRef]
37. Miao, Q.; Gong, Y.F.; Deng, R.J.; Wei, N.W. Impacts of the low frequency oscillation over the extra-tropics of the Northern Hemisphere on the extreme low temperature event in Northeast China in the winter of 2012/2013. *Chin. J. Atmos. Sci.* **2016**, *40*, 817–830. (In Chinese) [CrossRef]
38. Liu, Y.; Guo, P.W.; Feng, T. The relationship between winter persistent abnormal low temperature in North China and atmospheric low frequency oscillation activities. *Trans. Atmos. Sci.* **2016**, *39*, 370–380. (In Chinese) [CrossRef]
39. Jiang, Y.F.; Yao, S.X.; Wang, Y.Q.; Zhang, X.N. Intra-seasonal oscillation characteristics of low temperature events in January 2016. *J. Meteorol. Sci.* **2019**, *39*, 42–49. [CrossRef]
40. United Nations. *"Transforming Our World: The 2030 Agenda for Sustainable Development". United Nations General Assembly*; Seventieth Session; United Nations: New York, NY, USA, 2015.
41. United Nations. The Sustainable Development Goals Report 2018. 2018. Available online: https://unstats.un.org/sdgs/report/2018 (accessed on 20 June 2018).
42. Varotsos, C.A.; Cracknell, A.P. Remote Sensing Letters contribution to the success of the Sustainable Development Goals—UN 2030 agenda. *Remote Sens. Lett.* **2020**, *11*, 715–719. [CrossRef]
43. Robert, K.; Eugenia, K.; William, C. The NCEP–NCAR 50-year reanalysis: Monthly means CD-ROM and Documentation. *Bull. Am. Meteorol. Soc.* **2001**, *82*, 247–268. [CrossRef]
44. Torrence, C.; Compo, G.P. A Practical guide to wavelet analysis. *Bull. Am. Meteorol. Soc.* **1998**, *79*, 61–78. [CrossRef]
45. Murakami, M. Analysis of deep convective activity over the western Pacific and Southeast Asia. Part II: Seasonal and intraseasonal variation during the northern summer. *Meteorol. Soc. Jpn.* **1984**, *62*, 88–108. [CrossRef]
46. Maloney, E.D.; Hartmann, D.L. Frictional Moisture Convergence in a Composite Life Cycle of the Madden-Julian Oscillation. *J. Clim.* **1998**, *11*, 2387–2403. [CrossRef]
47. Mao, J.Y.; Chan, J.C.L. Intraseasonal variability of the South China Sea summer monsoon. *J. Clim.* **2005**, *18*, 2388–2402. [CrossRef]
48. Wei, F.Y. *Modern Climate Statistical Diagnosis and Prediction Techniques*; China Meteorological Press: Beijing, China, 2007.
49. Davis, R.E. Predictability of sea surface temperature and sea level pressure anomalies over the North Pacific Ocean. *J. Phys. Oceanogr.* **1976**, *6*, 249–266. [CrossRef]
50. Chen, W.Y. Fluctuations in Northern Hemisphere 700 mb height field associated with the Southern Oscillation. *Mon. Weather Rev.* **1982**, *110*, 808–823. [CrossRef]
51. Shi, N. *Multivariate Analysis Methods in Meteorological Research and Forecasting*, 2nd ed.; China Meteorological Press: Beijing, China, 2002.
52. Li, G.; Li, C.Y.; Tan, Y.K.; Bai, T. Principal modes of the boreal wintertime SSTA in the South Pacific and their relationships with the ENSO. *Acta Oceanol. Sin.* **2012**, *34*, 48–56.
53. Huang, W.Y.; Dong, W.; Shen, X.Y.; Guo, C.Y.; Li, X.F.; Liang, P. Isentropic vortex and thermodynamic analysis of a cold wave cooling process. *J. Meteorol. Sci.* **2020**, *40*, 769–781. [CrossRef]
54. Chang, C.P.; Lau, K.M. Northeasterly cold surges and near-equatorial disturbances over the winter MONEX area during December 1974. Part II: Planetary-scale aspects. *Mon. Wea. Rev.* **1980**, *108*, 298–312. [CrossRef]
55. Gao, S.T.; Tao, S.Y.; Ding, Y.H. Upper Wave-East Asian Jet Interaction during the Period of Cold Wave Outbreak. *Chin. J. Atmos. Sci.* **1992**, *16*, 718–724. [CrossRef]
56. Zhao, L.; Ding, Y.H. Potential vorticity analysis of cold air activities during the East Asian summer monsoon. *Chin. J. Atmos. Sci.* **2009**, *33*, 359–374. (In Chinese) [CrossRef]

57. Hu, B.W. Some Opinions about the "Potential Vorticity Thinking" and Its Applications. *J. Nanjing Inst. Meteorol.* **2003**, *26*, 111–115. [CrossRef]
58. Ding, Y.H.; Ma, X.Q. Analysis of isentropic potential vorticity for a strong cold wave in 2004/2005 Winter. *Acta Meteorol. Sin.* **2007**, *65*, 695–707. [CrossRef]
59. Xie, R.Q.; Liu, Y.D.; Zhu, J.S.; Meng, T. Analysis of Isentropic Potential Vorticity for an Extreme Cold Wave Event. *Meteorol. Sci. Technol.* **2019**, *47*, 312–321. [CrossRef]
60. Zhang, C.; Shen, X.Y.; Zhang, L.; Guo, C.Y.; Li, X.F. The dynamical cause of cold dome's intensification in a cold wave processes. *Plateau Meteorol.* **2021**, *40*, 394–402. [CrossRef]
61. Hoskins, B.J.; McIntyre, M.E.; Robertson, A.W. On the use and significance of isentropic potential vorticity maps. *Quart. J. Roy. Meteor. Soc.* **1985**, *111*, 877–946. [CrossRef]
62. Zhao, Q.G. An analysis with isentropic potential vorticity on a cold wave entering the Qinghai-Xizang Plateau. *Meteorol. Mon.* **1990**, *16*, 9–14. [CrossRef]
63. Zhao, Q.G. The characteristics of isentropic potential vorticity maps and their application to dynamical analysis and prediction. *Meteorol. Mon.* **1991**, *17*, 3–11. [CrossRef]
64. Jeong, J.H.; Kim, B.M.; Ho, C.H.; Chen, D.L.; Lim, G.H. Stratosphic origin of cold surge occurrence in East Asia. *Geophys. Res. Lett.* **2006**, *33*, L14710. [CrossRef]
65. Wu, Z.Y.; Li, H.J.; Zhao, H.J.; Yao, L.N.; Li, X.J. Disturbance features of mid-upper troposphere during a strong cold wave event revealed by isentropic potential vorticity analysis. *J. Mar. Meteorol.* **2017**, *37*, 84–91. [CrossRef]
66. Yu, F.S.; Lian, L.S.; Chu, C.C. Temporal-Spatial Variation Characteristics of Extreme Temperature Events in Shandong Province. *Meteorol. Sci. Technol.* **2017**, *45*, 843–850. [CrossRef]
67. Guo, X.Q.; Qian, L. Causal Analysis of a Late Frost Event in Eastern Hexi Corridor. *Meteorol. Sci. Technol.* **2018**, *46*, 369–373. [CrossRef]
68. Varotsos, C.A.; Mazei, Y.A. Future Temperature Extremes Will Be More Harmful: A New Critical Factor for Improved Forecasts. *Int. J. Environ. Res. Public Health* **2019**, *16*, 4015. [CrossRef]
69. Varotsos, C.A.; Efstathiou, M.N.; Cracknell, A.P. On the scaling effect in global surface air temperature anomalies. *Atmos. Chem. Phys.* **2013**, *13*, 5243–5253. Available online: https://www.researchgate.net/publication/258564811 (accessed on 6 August 2022). [CrossRef]
70. De Perez, E.C.; Van Aalst, M.; Bischiniotis, K.; Mason, S.; Nissan, H.; Pappenberger, F.; Stephens, E.; Zsoter, E.; Van Den Hurk, B. Global predictability of temperature extremes. Environ. *Res. Lett.* **2018**, *13*, 054017. [CrossRef]
71. Haiden, T.; Janousek, M.; Bauer, P.; Bidlot, J.; Dahoui, M.; Ferranti, L.; Prates, F.; Richardson, D.S.; Vitart, F. Evaluation of ECMWF forecasts, including 2014–2015 upgrades ECMWF Tech. *Memo* **2015**, *765*, 1–51. [CrossRef]
72. Varotos, C.; Cranknell, A.P.; Tzcanis, C.G. The exceptional ozone depletion over the Arctic in January–March 2011. *Remote Sens. Lett.* **2012**, *3*, 343–352. [CrossRef]
73. Krzyścin, J.W. Extreme ozone loss over the Northern Hemisphere high latitudes in the early 2011. *Tellus B Chem. Phys. Meteorol.* **2012**, *64*, 17347. [CrossRef]
74. Suo, C.N.; Tian, W.S.; Xie, F.; Luo, J.L.; Zhang, J.K. A comparative analysis of Arctic ozone depletion e- vents in the spring of 1997 and 2011. *Acta Meteorol. Sin.* **2017**, *75*, 492–505. [CrossRef]
75. Zhang, J.K.; Liu, W.; Han, Y.Y.; Wang, F.Y.; Xie, F.; Tian, H.Y. Progresses in Influence of Variations in Stratospheric Ozone on Tropospheric Climate. *J. Arid. Meteorol.* **2014**, *32*, 685–693. [CrossRef]
76. Hu, Y.Y. Possible Impact of Stratospheric Polar Ozone Depletion on Tropospheric Climate. *Acta Sci. Nat. Univ. Pekininsis* **2006**, *42*, 561–568. [CrossRef]
77. Lu, C.; Ding, Y. Analysis of isentropic potential vorticities for the relationship between stratospheric anomalies and the cooling process in China. *Sci. Bull.* **2015**, *60*, 726–738. [CrossRef]
78. Hu, Y.; Tung, K.K. Possible Ozone-Induced Long-Term Changes in Planetary Wave Activity in Late Winter. *J. Clim.* **2003**, *16*, 3027–3038. [CrossRef]
79. Hu, Y.; Tung, K.K.; Liu, J. A Closer Comparison of Early and Late-Winter Atmospheric Trends in the Northern Hemisphere. *J. Clim.* **2005**, *18*, 3204–3216. [CrossRef]